

Cite this: DOI: 00.0000/xxxxxxxxxx

From Polyhedra to Crystals: A Graph-Theoretic Framework for Crystal Structure Generation[†]Tomoyasu Yokoyama,^{*a} Kazuhide Ichikawa,^a and Hisashi Naito^bReceived Date
Accepted Date

DOI: 00.0000/xxxxxxxxxx

Crystal structures can be viewed as assemblies of space-filling polyhedra, which play a critical role in determining material properties such as ionic conductivity and dielectric constant. However, most conventional crystal structure prediction methods rely on random structure generation and do not explicitly incorporate polyhedral tiling, limiting their efficiency and interpretability. In this highlight, we introduced a novel crystal structure generation method based on discrete geometric analysis of polyhedral information. The geometry and topology of space-filling polyhedra are encoded as a dual periodic graph, and the corresponding crystal structure is obtained via the standard realization of this graph. We demonstrate the effectiveness of our approach by reconstructing face-centered cubic (FCC), hexagonal close-packed (HCP), and body-centered cubic (BCC) structures from their dual periodic graphs. This method offers a new pathway for systematically generating crystal structures based on target polyhedra, potentially accelerating the discovery of novel materials for applications in electronics, energy storage, and beyond.

1 Introduction

The essential parameters that determine a material properties are its composition and structure. Composition-based design—such as element substitution and alloying—has achieved significant success. This is largely due to the utility of the periodic table, which organizes chemical elements according to their properties and relationships, thereby guiding the selection of promising compositions.

For example, in the development of high-performance lithium-ion conductors like Li_3YCl_6 , one strategy to improve ionic conductivity is to substitute chlorine with a chemically similar element of lower electronegativity. The periodic table suggests bromine as a viable candidate, as it lies below chlorine and is less electronegative. Indeed, replacing Cl with Br yields Li_3YBr_6 , a compound

known to exhibit enhanced lithium-ion conductivity.¹

In contrast, crystal structure design remains far more challenging. A key reason is the absence of a systematic framework—akin to the periodic table—that captures the relationships among different crystal structures. As a result, the impact of structural modifications on material properties is often unclear. Compared to composition, structure-dependent properties such as ionic conductivity, dielectric response, and magnetism are less well understood. Overcoming this limitation could open a new avenue of materials discovery by enabling structure-based design, which may reveal functional materials beyond the reach of composition design alone.

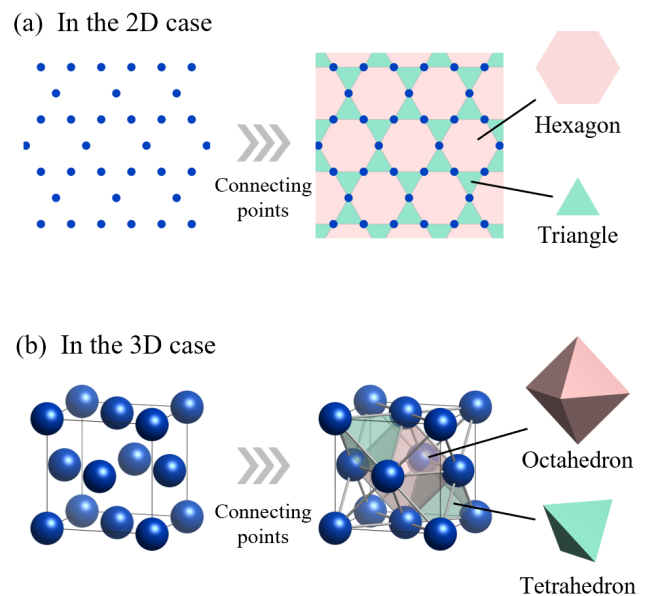


Fig. 1 Examples of crystal structures represented by periodic arrangements of lattice points: (a) in a two-dimensional plane forming a kagome lattice, and (b) in three-dimensional space forming a face-centered cubic (FCC) lattice with tetrahedral and octahedral tiling.

^a Green Transformation Division, Panasonic Holdings Corporation, Osaka, Japan. E-mail: yokoyama.tomoyasu@jp.panasonic.com

^b Graduate School of Mathematics, Nagoya University, Nagoya, Japan.

To understand relationships among crystal structures, it is essential to define their fundamental units. Just as prime numbers serve as the irreducible units of integers—since any integer can be expressed as a product of primes (e.g., $12 = 2 \times 2 \times 3$)—the basic units of composition are chemical elements. For instance, Li_3YCl_6 is composed of Li, Y, and Cl, and tuning their ratios or substituting elements forms the foundation of composition design.

So, what is the structural counterpart to an element in a crystal structure? We argue that it is the space-filling polyhedron. A crystal is essentially a periodic arrangement of unit cells, and each unit cell is composed of atoms arranged at the vertices of polyhedra that tile space without gaps. For instance, a two-dimensional periodic lattice can be connected by edges to form a graph—a kagome lattice—consisting of triangles and hexagons that tile the plane as shown in Figure 1a. These polygons serve as the minimal building blocks in 2D. Similarly, in 3D space, FCC structures can be regarded as tilings of space with tetrahedra and octahedra, where the vertices represent atomic positions as shown in Figure 1b. Thus, just as elements serve as the minimal units of composition, polyhedra can serve as the minimal units of crystal structures.

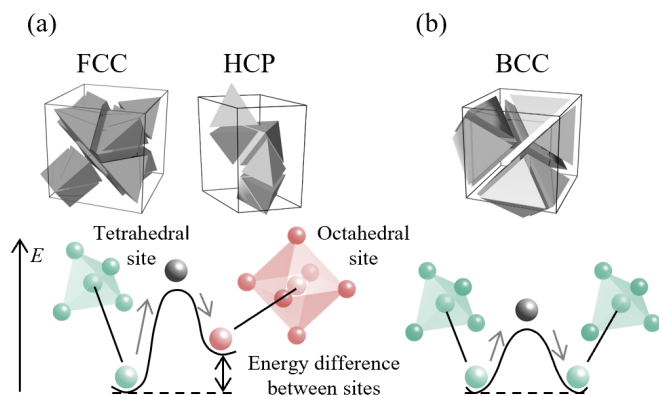


Fig. 2 Schematic of ionic conduction mechanisms in crystals with (a) FCC or HCP anion frameworks and (b) a BCC anion framework.

Importantly, the shape and connectivity of these polyhedra significantly influence material properties such as ionic conductivity. For example, it has been theoretically shown that ionic crystals with a BCC (body-centered cubic) anion framework exhibit higher ionic conductivity than those with FCC or HCP (hexagonal close-packed) frameworks.^{2,3} This arises from the polyhedral tiling of space: in FCC and HCP, the structure is composed of both tetrahedra and octahedra, while in BCC, the framework consists only of tetrahedra, as shown in Figure 2. As ions migrate through polyhedral centers, energy barriers arise from differences in polyhedral geometry. In systems where adjacent polyhedra differ in shape, the energy barrier is larger; where the polyhedra are same, the barrier is smaller. Hence, uniform tilings such as BCC tend to promote faster ion diffusion. Indeed, $\text{Li}_{10}\text{GeP}_2\text{S}_{12}$, which has a BCC-type anion framework, is one of the fastest lithium-ion conductors known.⁴

Despite the significance of polyhedra in governing properties,

there is currently no established method for designing crystal structures based on desired polyhedral arrangements. Most crystal structure prediction (CSP) approaches rely on random placement of atoms and lack control over polyhedral connectivity.^{5–8} Even in approaches where clusters are randomly arranged to maintain local motifs, generating structures with desired polyhedra remains difficult.⁹

To address this, we focus on a theory from discrete geometric analysis known as “standard realization,” proposed by Kotani and Sunada.¹⁰ This method uses graph theory and variational principles to derive crystal structures from periodic graphs by minimizing an energy functional. It has been used to predict new carbon structures with metallic behavior,^{11,12} as well as carbon structures with negative curvature.¹³ However, its application has been limited to specific systems such as carbon allotropes, and has not been extended to ionic or metallic crystals, nor has it been applied in the context of space-filling polyhedra.

In our recent work, we extended this theory to create a method for generating crystal structures from dual periodic graphs based on space-filling polyhedra.¹⁴ Conceptual diagram of our method is shown in Figure 3. In a dual periodic graph, the vertices represent the centers of space-filling polyhedra, and edges connect adjacent polyhedra. This dual representation enables direct encoding of polyhedral shape and connectivity. Given such a dual periodic graph, our method applies the theory of standard realization to generate a dual crystal structure, which is then transformed into a crystal structure using centroidal Voronoi tessellation (CVT). This enables the rational design of crystal structures from target polyhedral inputs, potentially accelerating the development of advanced ionic conductors and dielectric materials.

In this article, we first explain the fundamentals of the theory of standard realization and the concept of dual periodic graphs. Then, we describe the overall structure generation process, and demonstrate its application to FCC, HCP, and BCC structures. Finally, we discuss current challenges and prospects for this approach, including practical implementation steps and illustrative computational examples to guide readers interested in using this method.



Fig. 3 Conceptual diagram of our proposed crystal structure generation method based on dual periodic graphs and theory of standard realization. Reprinted with permission from ref. ¹⁴. Copyright 2024 American Chemical Society.

2 Standard Realizations

The theory of standard realization for crystal lattices, developed by Kotani and Sunada, formulates the crystal structure as a peri-

odic realization of a finite graph in Euclidean space.¹⁰ The theory is based on graph theory and the principle of energy minimization as shown in Figure 4. It models atomic positions as vertices connected by harmonic springs (a harmonic oscillator model), and seeks the configuration that minimizes the total elastic energy under the constraint of fixed unit cell volume. This optimized configuration is termed the “standard realization.” In the following, the method to construct a standard realization is briefly described. More detailed mathematical descriptions can be found elsewhere.^{10,15–17}

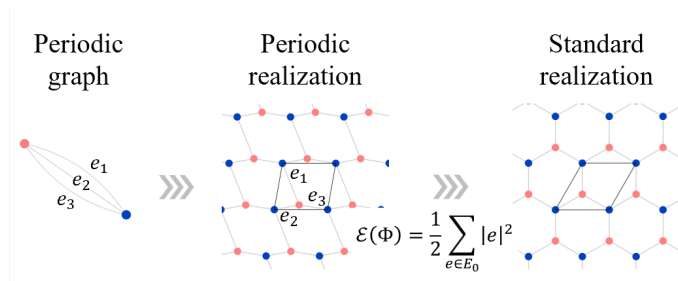


Fig. 4 Illustration of the theory of standard realization for crystal lattices. The most symmetric configuration is obtained by minimizing the harmonic oscillator energy under the constraint of fixed volume.

In this framework, a crystal lattice is represented by a periodic extension (covering) of a finite periodic graph $X_0 = (V_0, E_0)$, where V_0 and E_0 denote the sets of vertices and edges, respectively. A spanning tree $X_T = (V_0, E_T)$ is then extracted from X_0 , which is a subgraph that contains all vertices but no closed paths. The first Betti number b of the graph, representing the number of independent closed paths, is defined as $b = |E_0| - |E_T|$.

Each edge in E_0 is assigned a direction, and b linearly independent closed paths $\alpha_1, \alpha_2, \dots, \alpha_b$ are chosen to span the first homology group $H_1(X_0, \mathbb{Z})$. The b -dimensional real vector space $H_1(X_0, \mathbb{R})$ consists of linear combinations of these closed paths with real coefficients.

We then define an inner product $\langle e_j, e_k \rangle = \delta_{jk}$ for each pair of edges and compute two matrices: the $N \times b$ matrix $B = [\langle e_j, \alpha_k \rangle]$, and the $b \times b$ Gram matrix $G_0 = [\langle \alpha_j, \alpha_k \rangle]$. From these, we obtain the coefficient matrix $A = G_0^{-1}B$, which expresses each edge vector in terms of the chosen closed-path basis.

When the Betti number b exceeds the spatial dimension d , a projection onto a suitable d -dimensional subspace is required. This choice is made by selecting d out of the b closed paths, typically those forming a subspace that captures the symmetry of interest.

The lattice vectors $\mathbf{p}_x, \mathbf{p}_y, \mathbf{p}_z$ (in 3D) are constructed from the projection of G_0 , ensuring that the lengths and angles between basis vectors match the standard realization conditions. Once the edge vectors are determined, we compute the position of each vertex by tracing paths through the spanning tree, starting from a reference vertex placed at the origin. This yields the atomic positions for the unit cell.

Finally, the unit cell is extended periodically using the lattice vectors to generate the infinite crystal structure. Among all possible periodic realizations of the graph, the standard realization

has the highest spatial symmetry, faithfully reflecting the inherent symmetry of the underlying graph.

An illustrative example is shown in Figure 5, where different realizations of a hexagonal lattice are compared. The most symmetric case corresponds to the hexagonal tiling, which is obtained as the standard realization.

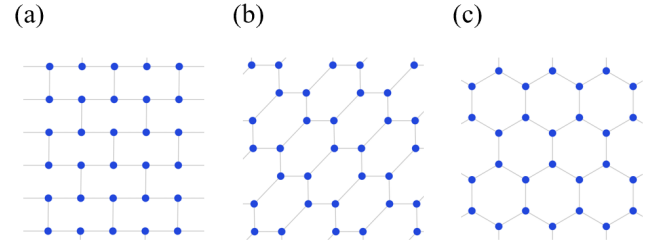


Fig. 5 Three different realizations of the same periodic hexagonal graph. Among them, (c) represents the standard realization with highest symmetry.

3 Dual Crystal Structure and Dual Periodic Graph

In general, a dual relationship refers to a correspondence between two paired entities—each being the dual of the other. For instance, an octahedron and a cube, or a Delaunay diagram and a Voronoi diagram, are well-known dual pairs. The dual of a dual structure returns to the original structure.

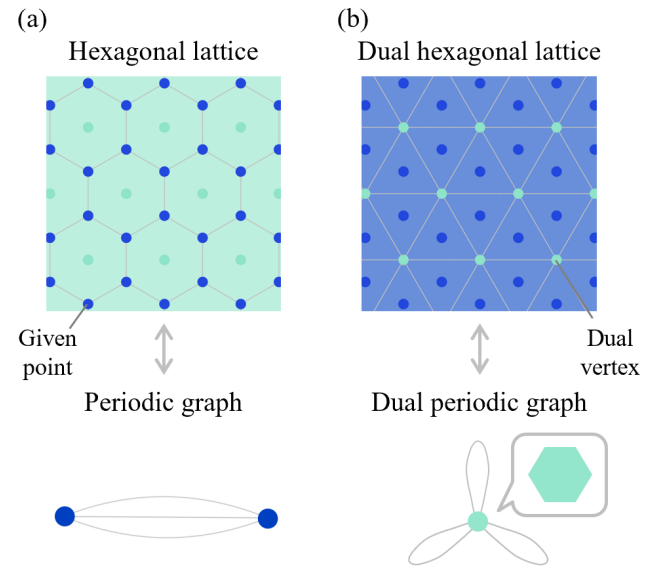


Fig. 6 Relationship between (a) a hexagonal lattice and its periodic graph, and (b) its dual structure and corresponding dual periodic graph.

Figure 6a shows an example of a two-dimensional (2D) crystal structure and its corresponding dual crystal structure. The structure illustrated is the hexagonal lattice. Here, a b -dimensional crystal structure is defined as a set of points that are periodically repeated in b -dimensional space. When edges are added between

specific points, this 2D structure forms a tessellation consisting of a hexagon. However, this polygonal composition is not apparent from the original periodic graph alone, which merely captures the connectivity of atomic sites.

To explicitly represent these tiles in a graph-theoretic framework, we introduce the concept of a dual crystal structure. A dual crystal structure is formed by connecting the centers of the space-filling polyhedra that constitute the original crystal structure. For instance, the dual of the hexagonal lattice is constructed by linking the centers of the hexagons that tile the plane.

The dual periodic graph is then defined as the periodic graph derived from this dual crystal structure. In the case of the hexagonal lattice, the dual vertex in Figure 6a has six connecting edges—corresponding to the number of edges in a hexagon.

Importantly, the original crystal structure and its dual share the same spatial symmetry when derived from a consistent polyhedral tiling. Therefore, the quotient group of periodicity, X/X_0 , remains invariant between the original and dual graphs.

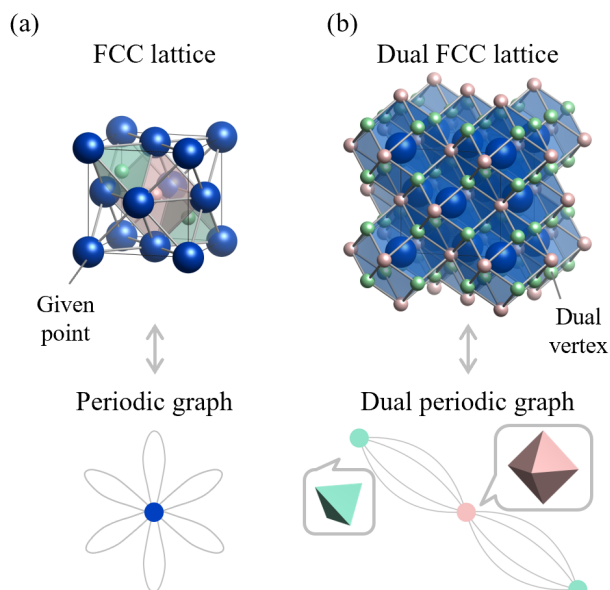


Fig. 7 Relationship between (a) FCC lattice and its periodic graph, and (b) its dual structure and corresponding dual periodic graph. Reprinted with permission from ref.¹⁴. Copyright 2024 American Chemical Society.

Just as in the 2D case, dual crystal structures and dual periodic graphs can also be defined in three-dimensional (3D) space. Figure 7 shows the FCC structure and its dual. By connecting adjacent atomic sites, the primitive cell of this 3D structure is seen to consist of two tetrahedra and one octahedron. The dual crystal structure is obtained by connecting the centers of these polyhedra. Although the periodic graph of the FCC structure does not reveal this polyhedral information, its dual periodic graph does reveal this: the green vertex connects to four edges and the red vertex to eight, corresponding to the number of faces in a tetrahedron and octahedron, respectively.

Thus, a dual periodic graph encodes the space-filling polyhedral framework of a crystal structure. By applying the standard

realization method to such graphs, one can reconstruct a dual crystal structure that inherently reflects the intended tiling geometry.

Although a dual graph is not uniquely determined for an abstract graph alone, it becomes uniquely defined when the spatial positions of graph vertices are specified. Our method begins by defining atomic bonds in the crystal structure, then forms a dual crystal structure based on these bonds and vertices. From this, the dual periodic graph is extracted. In other words, the dual periodic graph is defined by the geometry of a polyhedral tiling derived from the original structure.

To generate such tilings, we employ centroidal Voronoi tessellation (CVT), which partitions space by assigning regions to atoms based on proximity. In 2D, this yields polygons; in 3D, polyhedra. By treating the intersections of these regions as dual vertices, CVT enables bidirectional conversion between crystal and dual crystal structures.

4 Workflow

In this section, we explain the detailed procedure for generating a crystal structure from a given dual periodic graph (see Figure 8).

The input to the method is a dual periodic graph that encodes the shape and connectivity of space-filling polyhedra. The corresponding crystal structure is generated in eight steps. Steps 1 through 7 involve constructing a symmetric dual structure based on the theory of standard realization. Step 8 then converts this dual structure into a crystal structure via geometric transformation. These steps are conducted as follows.

1. Calculate the Betti number b from the given dual periodic graph X_0 . Here, b is equal to the number of edges in the graph $|E_0|$ minus the number of edges of maximal spanning trees $|E_T|$.
2. Define basis set $\{\alpha_j\}_{j=1}^b$ based on the number of selected closed paths corresponding to b obtained in step 1.
3. Define a basis set $\{\alpha_j\}_{j=1}^b$ based on the number of selected closed paths corresponding to the Betti number b obtained in Step 1. When $b > 3$, the choice of basis determines the three-dimensional subspace $\{\alpha_j\}_{j=1}^3$ onto which the structure will be projected, and the projection is taken onto the subspace defined by setting $\alpha_4 = \dots = \alpha_b = 0$.
4. Calculate the matrices G_0 , G , and A from the basis set $\{\alpha_j\}_{j=1}^b$ obtained in step 2 to project from the b -dimensional vector space to the 3D vector subspace. The matrices G_0 and G represent the conditions satisfied by the b - and 3D lattice vectors, respectively. The matrix A represents the basis of the edges in the b -dimensional vector space.
5. Define lattice vectors \mathbf{p}_x , \mathbf{p}_y , and \mathbf{p}_z such that the matrix G obtained in step 3 is satisfied. The lattice vectors can also be obtained by Cholesky decomposition of the matrix G .
6. Calculate the edge vectors $\{e_j\}_{j=1}^N$ from the matrix A obtained in step 3 and the lattice vectors \mathbf{p}_x , \mathbf{p}_y , and \mathbf{p}_z obtained in step 4.

7. Calculate the vertex vectors $\{v_k\}_{k=0}^{|V|-1}$ from the lattice vectors p_x , p_y , and p_z obtained in step 4 and the edge vectors $\{e_j\}_{j=1}^N$ obtained in step 5. The vertex vectors correspond to the primitive coordinates.
8. Generate a dual crystal structure from the lattice vectors p_x , p_y , p_z obtained in step 4 and the vertex vectors $\{v_k\}_{k=0}^{|V|-1}$ obtained in step 6.
9. Transform the dual structure obtained in step 7 into a crystal structure by CVT.

We begin by applying this process to a hexagonal lattice in two dimensions. This example illustrates the full procedure of standard realization. Subsequently, we apply the method to the dual periodic graph of the hexagonal lattice and demonstrate how the hexagonal lattice can be reconstructed from its dual representation.

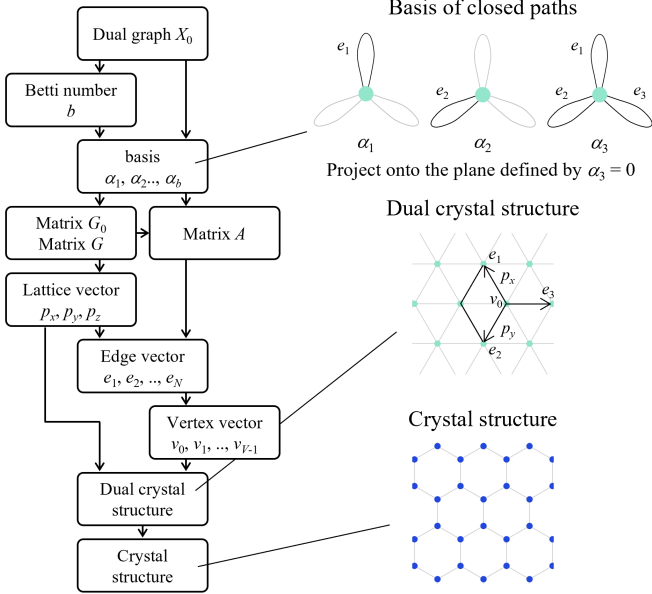


Fig. 8 Flowchart of the crystal structure generation method and the step-by-step generation of a hexagonal lattice from its dual periodic graph. Reprinted with permission from ref. ¹⁴. Copyright 2024 American Chemical Society.

4.1 Case Study: Hexagonal Lattice

This subsection presents the standard realization of a hexagonal lattice in two dimensions based on the original periodic graph—rather than the dual periodic graph—following a seven-step procedure that omits Step 8.

Step 1: We begin by computing the Betti number b , which represents the number of independent closed paths in the graph. It is given by the total number of edges $|E_0|$ minus the number of edges in a spanning tree $|E_T|$. For the original graph of the hexagonal lattice (Figure 6a), we have $|E_0| = 3$ and $|E_T| = 1$, resulting in $b = 2$. Since the structure is to be realized in two-dimensional space, the spatial dimension is $d = 2$.

Step 2: Next, we define the basis set based on the number of selected closed paths corresponding to $b = 2$. Let e_1 , e_2 , and e_3 denote the three directed edges of the graph, oriented from the left to the right vertex. Based on these, we define the basis set as

$$\alpha_1 = e_1 - e_3, \quad \alpha_2 = e_2 - e_3.$$

Step 3: Using this basis set, we compute the inner product matrix G_0 and the matrix B . Since the Betti number b equals the spatial dimension d in this case, we set $G = G_0$. The matrix G encodes the target geometry, specifically representing the inner products among the basis elements of the first homology group $H_1(X_0, \mathbb{Z})$. Accordingly, G determines the lengths and angles of the lattice basis vectors in the projected space. The matrix G is computed as follows:

$$G = G_0 = \begin{bmatrix} |\alpha_1|^2 & \langle \alpha_1, \alpha_2 \rangle \\ \langle \alpha_1, \alpha_2 \rangle & |\alpha_2|^2 \end{bmatrix} = \begin{bmatrix} 2 & 1 \\ 1 & 2 \end{bmatrix}. \quad (1)$$

The matrix B is constructed from the inner products between the edge vectors and the basis set as follows:

$$B = \begin{bmatrix} \langle e_1, \alpha_1 \rangle & \langle e_1, \alpha_2 \rangle \\ \langle e_2, \alpha_1 \rangle & \langle e_2, \alpha_2 \rangle \\ \langle e_3, \alpha_1 \rangle & \langle e_3, \alpha_2 \rangle \end{bmatrix} = \begin{bmatrix} 1 & 0 \\ 0 & 1 \\ -1 & -1 \end{bmatrix}. \quad (2)$$

The matrix $A = G^{-1}B$ expresses each edge vector in terms of the basis. By performing the matrix multiplication, we obtain:

$$e_1 = \frac{2}{3}\alpha_1 - \frac{1}{3}\alpha_2, \quad e_2 = -\frac{1}{3}\alpha_1 + \frac{2}{3}\alpha_2, \quad e_3 = -\frac{1}{3}\alpha_1 - \frac{1}{3}\alpha_2.$$

Step 4: we determine the lattice basis vectors p_x and p_y in 2D space so that they satisfy the geometric conditions encoded in G . Specifically, the following relationship must hold:

$$G = \begin{bmatrix} |p_x|^2 & \langle p_x, p_y \rangle \\ \langle p_y, p_x \rangle & |p_y|^2 \end{bmatrix}. \quad (3)$$

From this condition and the form of G obtained in Step 3, we observe that the standard realization of the hexagonal lattice yields translation vectors of equal length enclosing an angle of 60° . One possible set of lattice vectors satisfying this condition is:

$$p_x = \begin{bmatrix} \sqrt{2} \\ 0 \end{bmatrix}, \quad p_y = \begin{bmatrix} -1/\sqrt{2} \\ -\sqrt{3}/2 \end{bmatrix}.$$

Note that the choice of lattice vectors is not unique due to rotational and reflectional symmetry; they can also be computed using numerical methods such as Cholesky decomposition.

Step 5: Using the coefficient matrix A and the chosen lattice basis vectors, we can express the edge vectors explicitly as

$$e_1 = \begin{bmatrix} 1/\sqrt{2} \\ 1/\sqrt{6} \end{bmatrix}, \quad e_2 = \begin{bmatrix} 0 \\ \sqrt{2/3} \end{bmatrix}, \quad e_3 = \begin{bmatrix} -1/\sqrt{2} \\ -1/\sqrt{6} \end{bmatrix}.$$

Step 6: We place the reference vertex v_0 at the origin and define the other vertex positions as $v_0 + e_1$, $v_0 + e_2$, $v_0 + e_3$.

Step 7: We generate the crystal structure by periodically replicating the unit triangle defined by \mathbf{v}_0 , \mathbf{v}_1 , and \mathbf{v}_2 using the lattice vectors \mathbf{p}_x and \mathbf{p}_y . Replicating this triangle periodically using \mathbf{p}_x and \mathbf{p}_y yields the hexagonal lattice shown in Figure 6a.

While the construction is mathematically complete, the equivalence between this structure and a hexagonal tiling becomes visually evident only when the diagram is drawn.

4.2 Case Study: The Dual of Hexagonal Lattice

To illustrate how polyhedral shapes can be explicitly considered, we next apply the method to the dual periodic graph of the hexagonal lattice (Figure 6b). In this dual periodic graph, each vertex is connected to six edges, reflecting the six edges of a hexagon.

Step 1: We compute the Betti number b . This graph has $|E_0| = 3$ and $|E_7| = 0$, giving a Betti number of $b = 3$. Since the realization is in 2D space, the target spatial dimension is $d = 2$.

Step 2: Let e_1 , e_2 , and e_3 be directed edges forming three closed paths. If we let $\alpha_1 = e_1$, $\alpha_2 = e_2$, and $\alpha_3 = e_3$, the resulting 3D standard realization corresponds to a cubic lattice. However, here we take:

$$\alpha_1 = e_1, \quad \alpha_2 = e_2, \quad \alpha_3 = e_1 + e_2 + e_3,$$

and construct the standard realization in the 2D subspace spanned by α_1 and α_2 . Geometrically, this corresponds to projecting the cubic lattice onto its (111) plane.

Step 3: We compute the inner product matrix G_0 , the edge-closed path matrix B , and the coefficient matrix A as follows:

$$G_0 = \begin{bmatrix} 1 & 0 & 1 \\ 0 & 1 & 1 \\ 1 & 1 & 3 \end{bmatrix}, \quad B = \begin{bmatrix} 1 & 0 & 1 \\ 0 & 1 & 1 \\ 0 & 0 & 1 \end{bmatrix}, \quad A = G_0^{-1}B = \begin{bmatrix} 1 & 0 & 0 \\ 0 & 1 & 0 \\ -1 & -1 & 1 \end{bmatrix},$$

The three edge vectors in 3D become:

$$\mathbf{e}_1 = \alpha_1, \quad \mathbf{e}_2 = \alpha_2, \quad \mathbf{e}_3 = -\alpha_1 - \alpha_2 + \alpha_3.$$

Since G_0 describes the inner products of the 3D basis vectors before projection, we must recalculate the projected metric matrix G for the (111) plane. If we partition G_0 as:

$$G_0 = \begin{bmatrix} G_{11} & G_{12} \\ G_{21} & G_{22} \end{bmatrix}, \quad (4)$$

then the effective 2D metric is:

$$G = G_{11} - G_{12}G_{22}^{-1}G_{21}. \quad (5)$$

Here, G_{11} is a $d \times d$ matrix, G_{12} is $d \times (b-d)$, G_{21} is $(b-d) \times d$, and G_{22} is $(b-d) \times (b-d)$. In this case, G is given by

$$G = \frac{1}{3} \begin{bmatrix} 2 & -1 \\ -1 & 2 \end{bmatrix},$$

Step 4: Using the matrix G , we compute the projected lattice

vectors \mathbf{p}_x and \mathbf{p}_y in accordance with Eq. 3,

$$\mathbf{p}_x = \frac{1}{2} \begin{bmatrix} 1 \\ -\sqrt{3} \end{bmatrix}, \quad \mathbf{p}_y = \frac{1}{2} \begin{bmatrix} 1 \\ \sqrt{3} \end{bmatrix}.$$

Step 5: We reconstruct the edge vectors \mathbf{e}_1 , \mathbf{e}_2 , \mathbf{e}_3 as follows:

$$\mathbf{e}_1 = \mathbf{p}_x = \frac{1}{2} \begin{bmatrix} 1 \\ -\sqrt{3} \end{bmatrix}, \quad \mathbf{e}_2 = \mathbf{p}_y = \frac{1}{2} \begin{bmatrix} 1 \\ \sqrt{3} \end{bmatrix}, \quad \mathbf{e}_3 = -\mathbf{p}_x - \mathbf{p}_y = \frac{1}{2} \begin{bmatrix} -1 \\ 0 \end{bmatrix}.$$

Step 6 and 7: Using \mathbf{p}_x , \mathbf{p}_y , and a reference vertex \mathbf{v}_0 , we construct the dual crystal structure by periodically replicating the unit. The resulting structure is shown in Figure 6b.

Step 8: Finally, we apply CVT to the dual crystal structure to obtain the crystal structure. By placing new vertices at the centers of the triangles and connecting them appropriately, the original hexagonal tiling is recovered.

By employing a dual periodic graph, crystal structures can be systematically generated from prescribed polyhedral information, as demonstrated by the reconstruction of the hexagonal lattice via the standard realization method.

5 Applications to Representative Structures: FCC, HCP, and BCC

Following the same procedure used for two-dimensional lattices in the previous section, a three-dimensional crystal structure can be generated from a dual periodic graph. Here, we describe the specific steps using the FCC structure as an example. The dual periodic graph of the FCC structure is shown in Figure 10a.

The primitive unit cell of the FCC structure contains two interstitial tetrahedral sites and one interstitial octahedral site. In other words, the FCC structure can be viewed as a tiling of two tetrahedra and one octahedron. Each tetrahedron shares all of its faces with octahedra, and each octahedron shares all of its faces with tetrahedra. In the dual periodic graph, the green vertices (v_1 and v_2) are connected to four edges, and the red vertex (v_0) is connected to eight edges. These correspond to the number of faces of the tetrahedron and octahedron, respectively.

We now follow the procedure to generate the FCC structure from its dual periodic graph.

Step 1: We compute the Betti number b . The dual periodic graph has 8 edges and a spanning tree with 2 edges, resulting in $b = |E_0| - |E_T| = 8 - 2 = 6$. Since the structure is embedded in three-dimensional space, the dimension is $d = 3$.

Step 2: We define the basis set based on the number of selected closed paths corresponding to $b = 6$. Let the eight edges of the basic graph be denoted as e_1 through e_8 . We define the closed

path basis as follows:

$$\alpha_1 = e_1 - e_2,$$

$$\alpha_2 = e_1 - e_3,$$

$$\alpha_3 = e_1 - e_4,$$

$$\alpha_4 = e_1 - e_2 + e_5 - e_6,$$

$$\alpha_5 = e_1 - e_3 + e_5 - e_7,$$

$$\alpha_6 = e_1 - e_4 + e_5 - e_8.$$

These correspond to the closed paths illustrated in Figure 9.

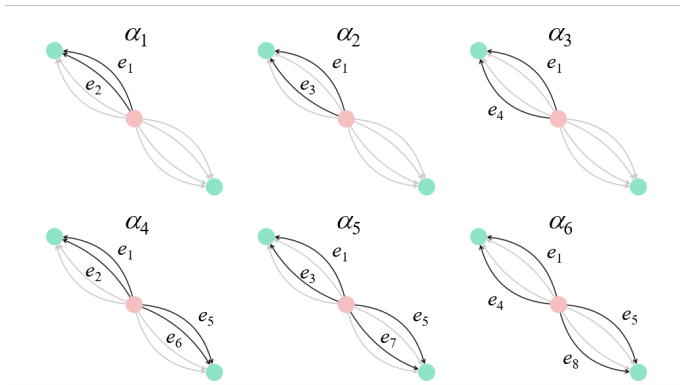


Fig. 9 Closed paths in the dual graph of the FCC structure that serve as bases for standard realization. Reprinted with permission from ref. 14. Copyright 2024 American Chemical Society.

Step 3: Using this basis, we compute the matrices G_0 , B , and A . The matrix G_0 is given by:

$$G_0 = \begin{bmatrix} 2 & 1 & 1 & 2 & 1 & 1 \\ 1 & 2 & 1 & 1 & 2 & 1 \\ 1 & 1 & 2 & 1 & 1 & 2 \\ 2 & 1 & 1 & 4 & 2 & 2 \\ 1 & 2 & 1 & 2 & 4 & 2 \\ 1 & 1 & 2 & 2 & 2 & 4 \end{bmatrix}.$$

The matrix B is:

$$B = \begin{bmatrix} 1 & 1 & 1 & 1 & 1 & 1 \\ -1 & 0 & 0 & -1 & 0 & 0 \\ 0 & -1 & 0 & 0 & -1 & 0 \\ 0 & 0 & -1 & 0 & 0 & -1 \\ 0 & 0 & 0 & 1 & 1 & 0 \\ 0 & 0 & 0 & -1 & 0 & 0 \\ 0 & 0 & 0 & 0 & -1 & 0 \\ 0 & 0 & 0 & 0 & 0 & -1 \end{bmatrix}.$$

Multiplying $G^{-1}B$ yields the matrix A :

$$A = \frac{1}{4} \begin{bmatrix} 1 & 1 & 1 & 0 & 0 & 0 \\ -3 & 1 & 1 & 0 & 0 & 0 \\ 1 & -3 & 1 & 0 & 0 & 0 \\ 1 & 1 & -3 & 0 & 0 & 0 \\ -1 & -1 & -1 & 1 & 1 & 1 \\ 3 & -1 & -1 & -3 & 1 & 1 \\ -1 & 3 & -1 & 1 & -3 & 1 \\ -1 & -1 & 3 & 1 & 1 & -3 \end{bmatrix}.$$

With Eqs. 4 and 5, the matrix G in 3D space is computed as:

$$G = \frac{1}{2} \begin{bmatrix} 2 & 1 & 1 \\ 1 & 2 & 1 \\ 1 & 1 & 2 \end{bmatrix}.$$

Step 4: We determine lattice vectors \mathbf{p}_x , \mathbf{p}_y , and \mathbf{p}_z satisfying:

$$G = \begin{bmatrix} |\mathbf{p}_x|^2 & \langle \mathbf{p}_x, \mathbf{p}_y \rangle & \langle \mathbf{p}_x, \mathbf{p}_z \rangle \\ \langle \mathbf{p}_y, \mathbf{p}_x \rangle & |\mathbf{p}_y|^2 & \langle \mathbf{p}_y, \mathbf{p}_z \rangle \\ \langle \mathbf{p}_z, \mathbf{p}_x \rangle & \langle \mathbf{p}_z, \mathbf{p}_y \rangle & |\mathbf{p}_z|^2 \end{bmatrix}. \quad (6)$$

An example set of lattice vectors is:

$$\mathbf{p}_x = \frac{1}{2} \begin{bmatrix} 1 \\ 0 \\ 1 \end{bmatrix}, \quad \mathbf{p}_y = \frac{1}{2} \begin{bmatrix} 1 \\ 1 \\ 0 \end{bmatrix}, \quad \mathbf{p}_z = \frac{1}{2} \begin{bmatrix} 0 \\ 1 \\ 1 \end{bmatrix}.$$

Step 5: Using the matrix A and the lattice vectors, we obtain the edge vectors \mathbf{e}_1 through \mathbf{e}_8 as:

$$\mathbf{e}_1 = \frac{1}{4}\mathbf{p}_x + \frac{1}{4}\mathbf{p}_y + \frac{1}{4}\mathbf{p}_z, \quad \mathbf{e}_2 = -\frac{3}{4}\mathbf{p}_x + \frac{1}{4}\mathbf{p}_y + \frac{1}{4}\mathbf{p}_z,$$

$$\mathbf{e}_3 = \frac{1}{4}\mathbf{p}_x - \frac{3}{4}\mathbf{p}_y + \frac{1}{4}\mathbf{p}_z, \quad \mathbf{e}_4 = -\frac{3}{4}\mathbf{p}_x + \frac{1}{4}\mathbf{p}_y - \frac{3}{4}\mathbf{p}_z,$$

$$\mathbf{e}_5 = -\frac{1}{4}\mathbf{p}_x - \frac{1}{4}\mathbf{p}_y - \frac{1}{4}\mathbf{p}_z, \quad \mathbf{e}_6 = \frac{3}{4}\mathbf{p}_x - \frac{1}{4}\mathbf{p}_y - \frac{1}{4}\mathbf{p}_z,$$

$$\mathbf{e}_7 = -\frac{1}{4}\mathbf{p}_x + \frac{3}{4}\mathbf{p}_y - \frac{1}{4}\mathbf{p}_z, \quad \mathbf{e}_8 = -\frac{1}{4}\mathbf{p}_x - \frac{1}{4}\mathbf{p}_y + \frac{3}{4}\mathbf{p}_z,$$

We then define vertex vectors from these edges.

$$\mathbf{v}_1 = \frac{1}{2} \begin{bmatrix} 1 \\ 1 \\ 1 \end{bmatrix}, \quad \mathbf{v}_2 = \frac{1}{2} \begin{bmatrix} -1 \\ 1 \\ -1 \end{bmatrix}, \quad \mathbf{v}_3 = \frac{1}{2} \begin{bmatrix} -1 \\ -1 \\ 1 \end{bmatrix}, \quad \mathbf{v}_4 = \frac{1}{2} \begin{bmatrix} 1 \\ -1 \\ -1 \end{bmatrix},$$

$$\mathbf{v}_5 = \frac{1}{2} \begin{bmatrix} -1 \\ -1 \\ -1 \end{bmatrix}, \quad \mathbf{v}_6 = \frac{1}{2} \begin{bmatrix} 1 \\ -1 \\ 1 \end{bmatrix}, \quad \mathbf{v}_7 = \frac{1}{2} \begin{bmatrix} 1 \\ 1 \\ -1 \end{bmatrix}, \quad \mathbf{v}_8 = \frac{1}{2} \begin{bmatrix} -1 \\ 1 \\ 1 \end{bmatrix}.$$

Step 6: Taking \mathbf{v}_0 as the origin, $\mathbf{v}_1 = \mathbf{v}_0 + \mathbf{e}_1$, and $\mathbf{v}_2 = \mathbf{v}_0 + \mathbf{e}_5$, the three vertex vectors are:

$$\mathbf{v}_0 = \frac{1}{2} \begin{bmatrix} 0 \\ 0 \\ 0 \end{bmatrix}, \quad \mathbf{v}_1 = \mathbf{v}_0 + \mathbf{e}_1 = \frac{1}{2} \begin{bmatrix} 1 \\ 1 \\ 1 \end{bmatrix}, \quad \mathbf{v}_2 = \mathbf{v}_0 + \mathbf{e}_5 = \frac{1}{2} \begin{bmatrix} -1 \\ -1 \\ -1 \end{bmatrix}.$$

Step 7: Using the lattice vectors \mathbf{p}_x , \mathbf{p}_y , and \mathbf{p}_z , and the vertex vectors \mathbf{v}_0 , \mathbf{v}_1 , and \mathbf{v}_2 , the dual crystal structure is defined. The structure can be written in VASP format as:

```
Dual FCC
1.0          #scale
1 0 1        #p_x
1 1 0        #p_y
0 1 1        #p_z
H           #element
3           #vertex number
Cartesian
0.0 0.0 0.0  #v_0
0.5 0.5 0.5  #v_1
-0.5 -0.5 -0.5 #v_2
```

Here, hydrogen atoms are placed at the dual vertices. Figure 10b shows the resulting dual crystal structure, which is composed of rhombic dodecahedra that tile the space.

Step 8: Finally, we convert the dual crystal structure to a crystal structure using CVT. By placing atoms at the centers of the rhombic dodecahedra and connecting them appropriately, we obtain the FCC crystal structure, as shown in Figure 10c. In the resulting structure, \mathbf{v}_0 corresponds to an octahedral center, and \mathbf{v}_1 and \mathbf{v}_2 correspond to tetrahedral centers. This demonstrates that our method correctly reproduces the FCC structure from its dual graph.

We applied the same procedure to the HCP and BCC structures. The dual periodic graph of HCP is shown in Figure 10d. The primitive unit cell of HCP contains four tetrahedral and two octahedral interstitial sites, meaning it consists of four tetrahedra and two octahedra. Unlike FCC, in the HCP structure, tetrahedra share faces with other tetrahedra, and octahedra share faces with other octahedra. The dual periodic graph contains four edges connected to each green vertex (v_2 – v_5), and eight edges connected to red vertices (v_0 and v_1), corresponding to tetrahedral and octahedral face counts.

The dual periodic graph of BCC is shown in Figure 10g. The primitive unit cell of BCC contains six tetrahedral interstitial sites. Unlike FCC and HCP, BCC consists solely of tetrahedra. The dual periodic graph features green vertices, each connected to four edges, corresponding to tetrahedral faces.

The resulting dual and crystal structures for HCP and BCC, generated by this method, are shown in Figure 10e–i. Although detailed procedures are omitted here, the generated crystal structures match the HCP and BCC structures, respectively. Thus, our method successfully reconstructs crystal structures from their dual periodic graphs. For more details on the construction process and implementation for HCP and BCC, please refer to ref.¹⁴.

6 Challenges and Outlook

In this study, we have demonstrated that FCC, HCP, and BCC structures can each be generated from their respective dual periodic graphs using our proposed methodology. Our method can be applied to generate a wide range of crystal structures—including undiscovered ones. However, our approach faces several technical challenges. In this section, we outline four key issues that must be addressed for practical and scalable applications of our method.

Combinatorial Explosion in Closed-Path Selection

A major challenge lies in selecting an appropriate set of closed paths when the Betti number b exceeds 3, which is typical for 3D periodic graphs. In such cases, the structure must be projected from a high-dimensional closed-path space onto 3D space, requiring a suitable selection of b linearly independent closed paths. For complex crystal structures, the number of possible closed-path combinations increases exponentially, making the selection process extremely challenging.

For instance, the dual periodic graph of the BCC structure contains 63 unique closed paths. To construct the correct dual BCC structure, one must select 7 closed paths (the Betti number), such as three 3-vertex closed paths, three 4-vertex closed paths, and one 6-vertex closed path. The total number of such combinations amounts to 407,680. Among them, only 128 combinations yielded the correct structure with the highest symmetry corresponding to the $\text{Im}\bar{3}m$ space group. The remaining combinations either produced structures with lower symmetry or failed to generate a valid crystal structure at all.

Although we identified a valid closed-path combination through trial and error, a general rule for optimal closed-path selection remains unknown. Even for highly symmetric structures with a small number of atoms in the unit cell, such as BCC, the combinatorial complexity makes it difficult to guarantee successful reconstruction. Solving this problem is essential for applying the method to more complex crystal structures. In future work, we aim to develop efficient algorithms to identify valid closed-path combinations.

Optimization of Atomic Site Configuration

The crystal structures generated by our method define only the spatial arrangement of atomic sites and do not specify atomic species at the sites. To apply this method to actual materials discovery, it is necessary to determine which atoms occupy which vertices. We recently developed a cost-efficient approach using Ising machine to solve the atomic site optimization problem.^{18,19} By applying such optimization technique to the structures generated by our framework, it becomes possible to predict novel, synthesizable materials through crystal structure design.

Generation of Low-Symmetry Structures

Our method inherently produces the most symmetric realization possible from a given graph. As a result, it is not directly suited for generating low-symmetry or distorted structures, which are

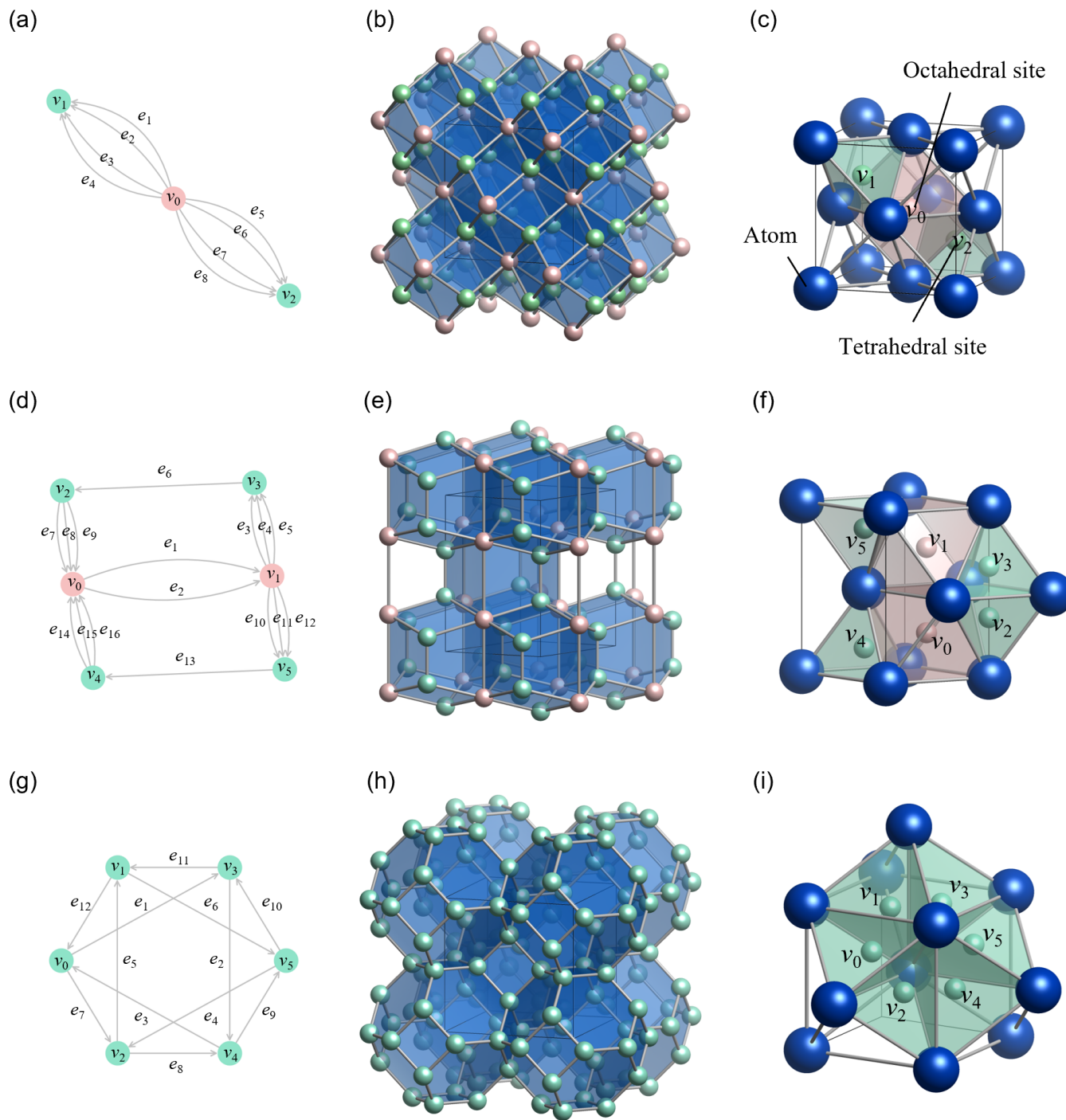


Fig. 10 Dual periodic graphs, dual crystal structures, and crystal structures reconstructed by our method for: (a–c) FCC, (d–f) HCP, and (g–i) BCC configurations. Reprinted with permission from ref.¹⁴. Copyright 2024 American Chemical Society.

often critical in functional materials.

To address this, our method can be combined with phonon analysis.²⁰ Using first-principles calculations or machine-learned interatomic potentials, we can perform phonon calculations on the high-symmetry structure generated by our method. By following unstable phonon modes, the structure can be systematically deformed into a lower-symmetry configuration. Since these optimization methods require a valid starting structure, our approach serves as an excellent generator of symmetric candidates for further analysis.

Deriving Dual Periodic Graphs from Given Polyhedra

To apply our method in a fully generative context—where crystal structures are predicted from abstract polyhedral inputs—it is necessary to first define a dual periodic graph from a given set of polyhedra. This involves determining the number of dual vertices and their connections based on the faces of adjacent polyhedra.

For example, given the shapes of polyhedra, one can determine which faces are compatible for joining, thereby constructing a dual periodic graph. Once all possible combinations of such dual periodic graphs are enumerated, our method can, in principle, generate all crystal structures derivable from that polyhedral set.

Finally, we compare our method based on discrete geometry with crystal structure prediction methods based on generative models, such as generative adversarial networks (GAN), variational auto-encoders (VAE), and diffusion models. Recent advances in generative models for CSP have shown promise in accelerating the discovery of novel materials.^{21,22} However, these methods typically require large volumes of training data to accurately predict lattice vectors and atomic positions. In contrast, our method—being grounded in graph theory and discrete geometry—requires no training data at all.

One limitation of the generative model is that it tends to generate structures that are less symmetric than the training data.²² In contrast, our method consistently produces highly symmetric structures, owing to its foundation in the theory of standard realization.

An intriguing opportunity lies in combining these two approaches: structures generated by our method could serve as templates for generative models. By performing elemental substitutions on such templates, a diverse set of hypothetical compounds can be created to enhance the extrapolative capability of generative models. This hybrid strategy may significantly accelerate the exploration of material space by blending the strengths of data-driven and structure-driven approaches.

7 Conclusion

In this highlight, we introduced a novel methodology for crystal structure generation based on polyhedral information using dual periodic graphs. By conceptualizing crystal structures as space-filling arrangements of polyhedra and constructing their corresponding dual graph representations, we developed a systematic framework grounded in discrete geometric principles.

This method was successfully applied to generate FCC, HCP, and BCC structures, demonstrating its capability to accurately reconstruct known crystal structures. The approach bridges the gap between abstract topological design and tangible crystal structure generation, offering a powerful tool for materials discovery.

Despite its potential, several challenges remain—particularly in automating the selection of closed-path bases. Nevertheless, this study represents a first step toward generating previously unknown crystal structures from target polyhedra. By enabling structure-driven materials development, our approach has the potential to identify highly functional materials that are difficult to discover through conventional composition-driven methods.

Data availability

No primary research results, software or code have been included and no new data were generated or analysed as part of this highlight.

Notes and references

- 1 T. Asano, A. Sakai, S. Ouchi, M. Sakaida, A. Miyazaki and S. Hasegawa, *Advanced Materials*, 2018, **30**, 1803075.
- 2 Y. Wang, W. D. Richards, S. P. Ong, L. J. Miara, J. C. Kim, Y. Mo and G. Ceder, *Nature Materials*, 2015, **14**, 1026–1031.
- 3 T. Yokoyama, K. Ichikawa, T. Naruse, K. Ohura and Y. Kaneko, *arXiv*, 2024, arXiv:2407.02838.
- 4 Y. Kato, S. Hori, T. Saito, K. Suzuki, M. Hirayama, A. Mitsui, M. Yonemura, H. Iba and R. Kanno, *Nature Energy*, 2016, **1**, 1–7.
- 5 C. W. Glass, A. R. Oganov and N. Hansen, *Computer physics communications*, 2006, **175**, 713–720.
- 6 Y. Wang, J. Lv, L. Zhu and Y. Ma, *Computer Physics Communications*, 2012, **183**, 2063–2070.
- 7 T. Yamashita, S. Kanehira, N. Sato, H. Kino, K. Terayama, H. Sawahata, T. Sato, F. Utsuno, K. Tsuda, T. Miyake *et al.*, *Science and Technology of Advanced Materials: Methods*, 2021, **1**, 87–97.
- 8 L. Chang, H. Tamaki, T. Yokoyama, K. Wakasugi, S. Yotsuhashi, M. Kusaba, A. R. Oganov and R. Yoshida, *npj Computational Materials*, 2024, **10**, 298.
- 9 T. Yokoyama, S. Ohuchi, E. Igaki, T. Matsui, Y. Kaneko and T. Sasagawa, *Journal of Physical Chemistry Letters*, 2021, **12**, 2023–2028.
- 10 M. Kotani and T. Sunada, *Transactions of the American Mathematical Society*, 2001, **353**, 1–20.
- 11 M. Itoh, M. Kotani, H. Naito, T. Sunada, Y. Kawazoe and T. Adschiri, *Physical Review Letters*, 2009, **102**, 055703.
- 12 T. Sunada, *Notices of the American Mathematical Society*, 2008, **55**, 208–215.
- 13 M. Tagami, Y. Liang, H. Naito, Y. Kawazoe and M. Kotani, *Cabon*, 2014, **76**, 266–274.
- 14 T. Yokoyama, K. Ichikawa and H. Naito, *Crystal Growth & Design*, 2024, **24**, 2168–2178.
- 15 H. Naito, SPECTRAL ANALYSIS IN GEOMETRY AND NUMBER THEORY, 2009, pp. 153–164.

- 16 T. Sunada, *Topological crystallography: With a view towards discrete geometric analysis*, Springer Japan, 2013, pp. 1–229.
- 17 H. Naito, *Trivalent Discrete Surfaces and Carbon Structures*, Springer Nature Singapore, Singapore, 2023, vol. 5.
- 18 K. Ichikawa, S. Ohuchi, K. Ueno and T. Yokoyama, *Physical Review Research*, 2024, **6**, 033321.
- 19 K. Ichikawa, G. Hayashi, S. Ohuchi, T. Yokoyama, K. N. Okada and K. Fujii, *arXiv*, 2025, arXiv:2503.09356.
- 20 A. Togo and I. Tanaka, *Physical Review B*, 2013, **87**, 184104.
- 21 T. Xie, X. Fu, O.-E. Ganea, R. Barzilay and T. Jaakkola, *arXiv*, 2021, arXiv:2110.06197.
- 22 C. Zeni, R. Pinsler, D. Zügner, A. Fowler, M. Horton, X. Fu, Z. Wang, A. Shysheya, J. Crabbé, S. Ueda *et al.*, *Nature*, 2025, 1–3.